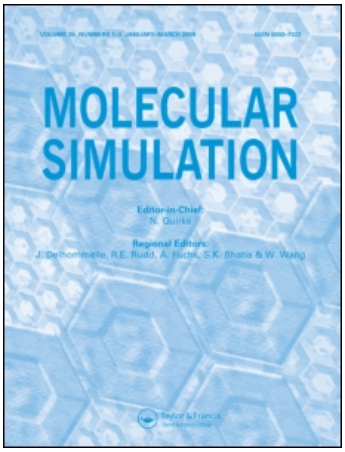

Molecular Simulation
Publication details, including instructions for authors and subscription information:
http://www.informaworld.com/smpp/title~content=t713644482

Assessment of the convergence of molecular dynamics simulations of lipopolysaccharide membranes

T. A. Soares[a]; T. P. Straatsma[a]
[a] Pacific Northwest National Laboratory, Richland, WA, USA

To cite this Article Soares, T. A. and Straatsma, T. P.(2008) 'Assessment of the convergence of molecular dynamics simulations of lipopolysaccharide membranes', Molecular Simulation, 34: 3, 295 — 307
To link to this Article: DOI: 10.1080/08927020701829880
URL: http://dx.doi.org/10.1080/08927020701829880

Molecular Simulation
Vol. 34, No. 3, March 2008, 295–307

Taylor & Francis
Taylor & Francis Group

Assessment of the convergence of molecular dynamics simulations of lipopolysaccharide membranes

T.A. Soares and T.P. Straatsma*

Pacific Northwest National Laboratory, Richland, WA, USA

(Received 15 October 2007; final version received 17 November 2007)

The outer membrane of Gram-negative bacteria is composed of a phospholipid inner leaflet and a lipopolysaccharide (LPS) outer leaflet. The chemical structure of LPS results in an asymmetric character of outer membranes that has been shown to play an important role in the electrical properties of porins, low permeability and intrinsic antibiotic resistance of Gram-negative bacteria. Atomistic molecular dynamics simulations of two different configurations of the outer membrane of *Pseudomonas aeruginosa* under periodic boundary conditions were carried out in order to (1) validate model-derived properties against the available experimental data, (2) identify the properties whose dynamics can be sampled on nanosecond timescales, and (3) evaluate the dependence of the convergence of structural and dynamical properties on the initial configuration of the system, within the chosen force field and simulation conditions. Because the relaxation times associated with the motions of individual LPS monomers in outer membranes are very long, the two initial configurations do not converge to a common ensemble of configuration on the nanosecond time scale. However, a number of properties of the outer membrane that will significantly impact the structural and internal dynamics of transmembrane proteins, most notably the electrostatic potential and molecular density, do converge within the simulated time scale. For these properties, a good agreement with the available experimental data was found. Such a molecular model, capable of accounting for the high asymmetry and low fluidity characteristics of outer membranes provides a more appropriate environment for atomistic simulations of outer membrane proteins.

Keywords: lipopolysaccharide structure; outer membrane; S^2 order parameters; area per lipid molecule; transmembrane potential; asymmetric bilayer

1. Introduction

Lipopolysaccharide (LPS) is the major component of the outer membrane of Gram-negative bacteria. This class of molecules provides an asymmetric character to outer membranes with the LPS monolayer forming the outer leaflet and phosphatidylethanolamine (PE) molecules forming the inner leaflet. Because of its specific physicochemical properties, LPS plays a fundamental role in the formation and function of the outer membrane, contributing to its low permeability and antibiotic resistance [1]. LPS also contributes to the functional lipid environment for outer membrane proteins and is essential for their correct function [2]. As the main virulence factor associated with Gram-negative bacteria, LPS molecules exert a variety of biological effects in mammals, in particular the production of proinflammatory cytokines [3,4]. Under conditions of excessive or systematic exposure to LPS – particularly when it enters the blood stream – a systemic inflammatory reaction can occur, leading to sepsis, septic shock, multi-organ failure and death. Among Gram-negative bacteria, *Pseudomonas aeruginosa* is a major opportunistic human pathogen with inherent resistance against antibiotics and making infections difficult to treat [5].

LPS from different species have a common general architecture with three distinct regions (Figure 1; [4]). Lipid-A consists of two glucosamine–phosphate moieties bound to lipid chains that can vary in length and number depending on the bacterial strain. This region is the endotoxically active part of the molecule. Covalently linked to Lipid-A is a core oligosaccharide that can be divided into inner and outer core region. The inner core contains a high proportion of the unusual sugars 2-keto-3-deoxy-D-manno-octulosonic acid (KDO) and L-glycero-D-manno-heptose (HEP) whereas the outer core consists of common sugars such as hexoses and hexamines. Onto this, a polymer of repeating saccharide subunits called *O*-antigen is attached. These oligosaccharides, typically hexoses, determine the serotype specificity of LPS molecules. The *O*-antigen region is often truncated or lacking altogether in particular strains [4]. Overall, structural variability is the lowest in the Lipid-A region (conservative structure), higher in the core oligosaccharide and highest in the *O*-polysaccharide chain.

*Corresponding author. Email: tps@pnl.gov

ISSN 0892-7022 print/ISSN 1029-0435 online

DOI: 10.1080/08927020701829880
http://www.informaworld.com

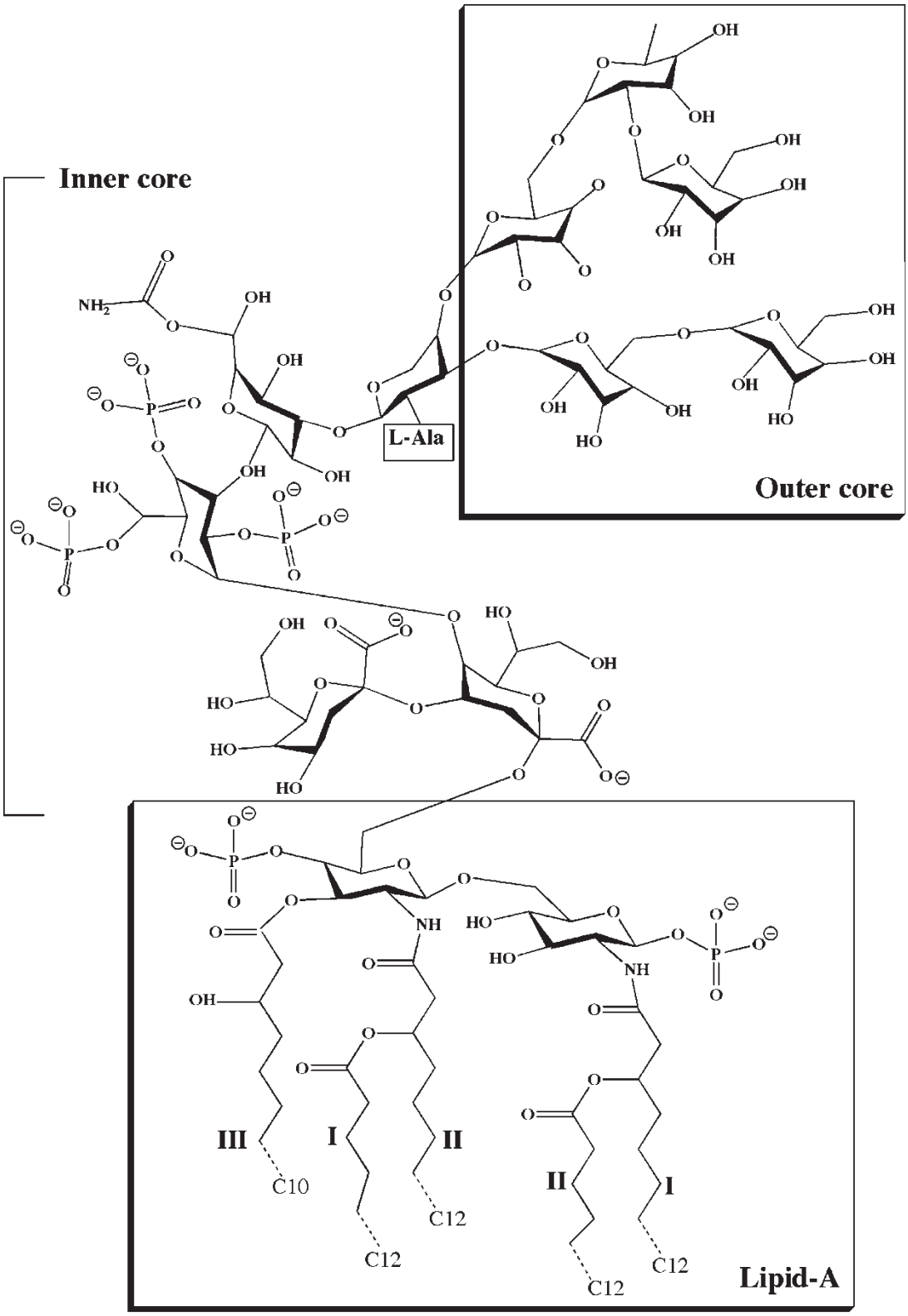

Figure 1. Chemical structure of the LPS molecule of *P. aeruginosa*.

The variability of the core oligosaccharide and the *O*-antigen between different bacterial stains and genera indicates that the main role of the sugar moiety is as epitopes for antibody binding and as steric hindrance for hydrophobic drugs (i.e. outer membrane impermeability).

In *P. aeruginosa* two types of *O*-specific chains have been identified [6]. The presence or absence and type of *O*-specific chain appear to be environmentally controlled, and provides a means of classification of the LPS membrane: A+B+, A−B−, A+B− and A−B+. The classification A − B − represents the so-called rough LPS which has the strongest biological activity. To a large extent, the LPS membrane stability is due to the multiple phosphoryl substituents in the core region. *P. aeruginosa* is among the Gram-negative bacteria with the most highly phosphorylated saccharides in the inner core region, with three phosphate groups on the C2, C4 and C6 positions of the inner core heptose [7,8]. These, together with the phosphate groups on both proximal and distal glucosamine head groups of Lipid-A, are essential for the integrity of the membrane through strong ionic interactions between the negatively charged core oligosaccharide and divalent counter ions [8].

The unique features of the supramolecular structure and conformation of LPS molecules determine the physical and chemical properties of the outer membrane such as fluidity of the Lipid-A acyl chains and backbone charge density and have implications for its biological function [1]. Currently, experimental atomic-level three-dimensional structures of LPS membranes are not available, in part due to the difficulty to manipulate such heterogeneous systems and to manufacture aligned LPS multi-bilayer stacks necessary for good quality diffraction measurements [9]. Molecular dynamics (MD) simulations can provide detailed microscopic information on biological macromolecules not always accessible from experiments [10]. By comparing such simulations against the available experiments, it is then possible to correlate atomic–scale interactions and fluctuations with experimental kinetics and thermodynamics measurements. We have previously developed a molecular model [11] for the rough LPS membrane of *P. aeruginosa* based on the chemical composition information from mass spectroscopy [7]. MD simulations in explicit solvent were undertaken for an outer membrane slab consisting of 16 LPS and 40 PE molecules, and the results were validated against available experimental data [11].

Finite computational resources impose significant limitations on both the length scales and the time scales accessible by atomistic simulations using an explicit representation of the solvent molecules. A fundamental question when interpreting the results of these simulations is whether the simulated system has been sampled long enough to enable fair comparison with experiment [10]. This question is particularly pertinent for MD simulations of LPS membranes. Due to their structural complexity, consisting of a highly charged polysaccharide surface and a fluid hydrophobic lipid core, the lateral diffusion of LPS monomers in outer membranes is very slow with a diffusion coefficient of $2.0 \pm 0.9 \times 10^{-10}\,\mathrm{cm^2\,s^{-1}}$ [12]. For comparison, typical diffusion coefficients for phospholipids in membrane bilayers are of the order of $10^{-8}\,\mathrm{cm^2\,s^{-1}}$ [13]. As result, the convergence of different properties of LPS membranes occurs at different time scales during a MD simulation and for some properties full convergence may not be achieved on a nanosecond timescale. Yet, a molecular level characterisation of the specific interactions that determine the structure, integrity and dynamics of the LPS outer membrane is essential for the understanding of the effect of these membranes on small molecule binding, transmembrane protein stability and material transport across these membranes through channel proteins and porins. Current MD simulations of outer membrane proteins reported in the literature represent the membrane environment as phospholipid bilayers. Although this is a valid approximation to the conditions present in many *in vitro* studies of such systems, investigation of their behaviour *in vivo* requires a more realistic representation of the outer membrane environment [2,14,15].

In order to evaluate the ability of the LPS molecular model to reproduce known experimental properties of outer membranes, MD simulations in explicit solvent were performed for two different initial configurations of an outer membrane slab formed by 64 LPS and 140 dipalmitoylphospho-ethanolamine (DPPE) molecules. Analysis of the MD-derived time trajectories was carried out with three goals: (1) validation of sampled properties, such as atomic distributions, area per lipid headgroup, order parameters S^2 and electrostatic potential gradient across the membrane against the available experimental data; (2) identification of those properties whose dynamics can be sampled on nanosecond timescales, and (3) evaluation of the dependence of the convergence of structural and dynamical properties on the initial configuration of the system, within the chosen force field and simulation conditions.

2. Material and methods

2.1 Construction and compaction of the LPS membrane

The LPS membrane consists of a highly charged surface and a fluid lipid core with diffusion coefficients in the range of $10^{-10}\,\mathrm{cm^2\,s^{-1}}$ [12]. In order to balance the charged functional groups on the saccharide units of the outer core, counter-ions (six Ca^{2+} per LPS molecule) are required. These characteristics make the construction

and equilibration of a fully atomistic configuration of the LPS membrane a non-trivial task. As a result, the conventional approaches used to construct and equilibrate phospholipids bilayers are inadequate for LPS membranes. We have developed a multiple-step protocol to construct and equilibrate the LPS membrane as described here:

(1) LPS layer assembly – geometry-optimised LPS molecules plus associated counter-ions (LPS cluster) are added one by one on a regularly spaced grid.
(2) DPPE layer assembly – the same procedure is used for the phospholipid layer, ensuring that the number of acyl chains in the latter is equivalent to those in the LPS layer.
(3) Membrane assembly – LPS molecules are assembled into the membrane on a regular two-dimensional grid with all LPS molecules placed either identically aligned (LPS_a) or randomly rotated around the molecular axis normal to the plane of the membrane (LPS_r).
(4) Membrane collapsing – each of the LPS clusters are successively moved within plane of the membrane towards the center of the simulation box as far as possible without causing atomic overlap with other LPS clusters. This process is repeated in an iterative fashion until the largest distance an LPS cluster can move falls below a preset value. During this process the relative atomic distances within an LPS cluster are not allowed to change. Several iterations are required until each cluster interacts favorably to a neighboring unit leading to a more compact configuration of the system.
(5) Membrane relaxation – through application of high-pressure anisotropic coordinate scaling at 1.025×10^9 Pa, and scaling of atomic charges by a factor of 0.5, the physical gaps between each sub-unit were gradually eliminated. The initial pressure of 1.025×10^8 Pa was slowly decreased to 1.025×10^5 Pa and the atomic charge were slowly rescaled to their correct values. During this process all atoms are allowed to move, although restraint potentials were applied to ensure that the overall orientation of the LPS and phospholipid molecules remains perpendicular to the plane of the membrane. These MD simulations were run at 50 K for 5 ns with a 1 fs time step and a cutoff of 1.4 nm. Once the density of the LPS membrane approached the experimental value, the system was solvated and equilibrated without additional restraints.

This approach is easily adapted to allow the construction of LPS aggregates around outer membrane proteins. For that, it suffices to replace some LPS units by the outer membrane protein before Step 4.

2.2 Molecular dynamics simulation

The outer membrane fragment of *P. aeruginosa* simulated in this study consisted of monolayers of 64 LPS molecules and 160 PE molecules. After the described setup of the system, all subsequent simulations were carried out under periodic boundary conditions, such that the membrane consisted of a periodic layer of LPS molecules exposed to an exterior aqueous environment and a PE layer also exposed to water, representing the periplasmic space. In order to minimise interactions between the LPS saccharide units on the top of the membrane and periodic images of its bottom lipids, a large box size perpendicular to the membrane was used and anisotropic pressure scaling was applied in that dimension. The dimensions of the simulation volume fluctuated around of $8.3 \times 8.3 \times 14.2$ nm. The SPC (Single Point Charge)/E water model was used [16].

MD simulations were carried out in the NPT ensemble with a time step of 1 fs in the equilibration phase and 2 fs in the production phase to integrate the equations of motion based on the leapfrog algorithm [17]. Before the equilibration phase, the solvent was energy minimised using the steepest descent optimisation algorithm. The equilibration procedure consisted of thermalisation of the solvent, with the solute atoms fixed, for 250 ps at 298.15 K, followed by minimisation of all solute atoms, keeping the solvent coordinates fixed. Subsequently, the temperature of the entire system was raised from 0 to 298.15 K in 250 ps increments of 50 K. The temperatures of solute and solvent were controlled separately by coupling them to a Berendsen thermostat [18] with a relaxation time of 0.1 and 0.4 ps, respectively. The pressure was maintained at 1.025×10^5 Pa by means of anisotropic coordinate scaling with a relaxation time of 0.4 ps. The bond lengths between hydrogen and heavy atoms were constrained by using the SHAKE algorithm [19] with a tolerance of 10^{-4} nm. A cutoff of 1.0 nm was used for all non-bonded interactions, and long-range electrostatic interaction contributions were evaluated using the smooth particle mesh Ewald method [20] with 64 grid points per dimension.

To ensure the integrity of the membrane during the equilibration phase, restraining potentials were applied to keep the *N*-acetyl-glucosamine residues of all LPS molecules in the plane of the membrane. Similar restraining potentials were also applied to the phosphate groups of the PE molecules. Additional restraining potentials were applied to the lipid chains of the PE and LPS molecules to keep them aligned in a direction normal to the plane of the membrane. The restraint potentials were gradually removed during the first 3.25 ns

of equilibration at 298.15 K and 1.025×10^5 Pa. No restraints were used during the production phase. Data production was carried out for 10 ns and configurations of the trajectory were recorded every 0.2 ps. All simulations were performed with the NWChem program [21].

2.3 Analyses

Analyses were performed for the full 10 ns trajectories generated during data production. Monitored properties included the distribution of functional groups along the axis normal to the plane of the LPS membrane, area per lipid/LPS molecule, carbon–deuterium order parameters S_{CD} of lipid tails, the dependence of the degree of randomisation of the membrane on the initial configuration and the electrostatic potential across the membrane. The area per lipid/LPS molecule was calculated from the lateral box dimensions divided by the number of lipids/LPS molecules in the corresponding leaflet. The carbon–deuterium order parameter S_{CD} is defined as:

$$S_{CD}(i) = \frac{1}{2}\cdot(3\langle\cos^2\theta\rangle - 1) \quad (1)$$

where θ is the angle between the carbon–deuterium vector of the ith methylene group in the lipid and the longitudinal axis of the system and the angular brackets denote ensemble averaging. If the lipids chains are perfectly ordered in the membrane, the angle between the C–D vectors in the acyl chain and the bilayer normal will be 90°. This situation corresponds to $S_{CD} = -0.5$. A value of $S_{CD} = 0$ corresponds to an orientation of the C–D vector that is either permanently at an angle of 0° or random. Because lipid tails in membranes are on average aligned along the bilayer normal, typical S_{CD} values are between 0 and -0.5, with -0.5 indicating maximum order. S_{CD} values are usually reported as $-S_{CD}$ or $|S_{CD}|$.

One of the primary objectives of this study is to evaluate the extent to which the initial configuration determines the degree of randomisation of the membrane. The averaged normalised dot product of each possible pair of vectors v_i defined from the phosphorous atom on the *N*-acetyl-glucosamine residue to the phosphorous atom on the neighbour *N*-acetyl-glucosamine residue can be defined as a quantitative measure of this randomisation of the lipid-A head groups of the LPS membrane.

$$\bar{\chi} = \frac{1}{N(N-1)}\sum_{i=1}^{N-1}\sum_{j=i+1}^{N}\frac{v_i\cdot v_j}{|v_i||v_j|} \quad (2)$$

A completely randomised configuration will lead to an average value of the degree of randomness $\bar{\chi}$ to be zero. For a configuration in which all LPS molecules are aligned identically, this quantity is expected to be close to one.

The electrostatic potential across the LPS membrane was calculated from the partial atomic charges used in the simulations. The electrostatic potential at a given coordinate in space x, $\phi(x)$, is defined as the work necessary to bring a unit positive charge from infinity to x. The electrostatic interaction energy between a point charge q located at x and the molecule is equal to $q\phi(x)$. In these calculations, edge-related artifacts were avoided by using periodic boundary conditions. The grid was extended up to 1.0 nm beyond the solute atoms in the transmembrane axis and the water molecules removed for the electrostatic potential calculation. Electrostatic potential calculations were carried out by using a grid of ten points per nm together with a 2.0 nm cutoff. A total of 5000 structures regularly sampled along the trajectory files were used for the electrostatic calculations.

Analyses of molecular trajectories were carried out using the data intensive trajectory analysis capabilities of the DIANA (Data Intensity Analysis) software [22]. This code is designed to take advantage of the large aggregate memory available on large massively parallel computer systems. The current capabilities include a wide range of geometric properties, root mean square deviation and fluctuations, Ramachandran distributions, principal component analysis for essential dynamics analysis, electrostatic potentials, potential gradients and deuterium order parameter calculations. A number of the analysis tools have been implemented as part of the work described here. The efficiency of DIANA is based on the parallel reading of trajectory data, filtering to reduce memory requirements and keeping all required data in core for a compete range of analyses to be carried out. Routine simulations of large molecular systems typically produce between 10 GB and 1 TB of data, which is easily held in the aggregate memory of large parallel computers. Good scalability with number of processors and with size of the data sets is achieved from this he combination of using the parallel I/O capabilities and the fact that only a single pass through the data file needs to be made.

3. Results and discussion

3.1 Thermodynamic properties

Most thermodynamic quantities in the LPS_a and LPS_r simulations converged during the 5 ns equilibration period, after which they fluctuate around certain values with small amplitudes. The average total energies, together with their kinetic, covalent, van der Waals and electrostatic components corresponding to the two simulations are presented in Table 1. Bulk properties such as density were well converged after the 5 ns of equilibration (Figure 2(D)). Likewise, the individual contributions to the potential energy from non-bonded

Table 1. Average energies calculated from the MD simulations of the aligned and random configurations of the LPS membrane.

Energy/10^3 (kJ mol^{-1})	Aligned configuration	Random configuration	Difference
E_{tot}	−1936 ± 3	−1920 ± 2	−16
E_{kin}	279.2 ± 0.6	279 ± 0.6	−0.2
E_{pot}	−2215 ± 3	−2219 ± 2	−4
E_S	−655 ± 0.8	−666 ± 0.8	−1
E_{SW}	−107 ± 3	−96 ± 3	−11
E_W	−1506 ± 1	−1504 ± 0.8	−2

Note: Different quantities are averaged over the last 10 ns of simulation and reported with standard deviation values. The energies reported for the random configuration ensemble were corrected for the differences of 591 water molecules between the two systems. The total energy, potential energy and solvent–solvent interaction energy were corrected by subtracting 591 times the enthalpy of a bulk water molecule (41.5 kJ mol^{-1}; [16]). The kinetic energy was corrected for each of the degrees of freedom at 298.15 K of the 591 water molecules. Energy differences are given by subtracting the averages for the aligned configuration from the randon configuration simulations.

intra-solute interactions converged during the equilibration phase. The potential energy E_{pot} (Figure 2(A)) exhibited slower convergence. This term is the sum of the solute–solute interaction energy E_S, the solute–solvent interaction energy E_{SW} and the solvent–solvent interaction energy E_W. The solute–solute energy E_S converged after 4 ns of equilibration (Figure 2(B)) whereas the solvent–solvent interaction energy E_W converged around 1–2 ns of the production phase (Figure 2(D)). However, the solute–solvent interaction energy E_{SW} required longer simulation times before reaching convergence (Figure 2(D)) and determines the convergence behaviour of the potential energy E_{pot}.

3.2 *Structural dynamics*

The distribution of atoms along the direction normal to the membrane (z-axis) for the LPS_a and LPS_r simulations at different time intervals are presented in Figure 3. The intervals correspond to the first and last 2.5 ns as well as the whole 10 ns of simulation after the equilibration. The LPS_a and LPS_r simulations exhibited a very similar profile for most of the functional groups considered, without significant differences between the two simulations. A different pattern is observed for water molecules whose distribution along the z-axis differs substiantially between the two simulations (Figure 3(D)). The LPS_a simulation showed a significantly faster diffusion of water molecules into the polysaccharide layer compared to the LPS_r simulation in the same simulation time. By integrating the area defined by the distribution curve for the region corresponding to the inner- and outer-core, the LPS_a configuration is around 10% more hydrated than the LPS_r after 10 ns of simulation. Comparison of the water distribution for different time intervals of the same simulation shows an increase of the total number of water molecules absorbed into the LPS membrane (Figure 3(D)). This indicates that the diffusion of interfacial water molecules into the membrane surface is slow as is also shown by the slow

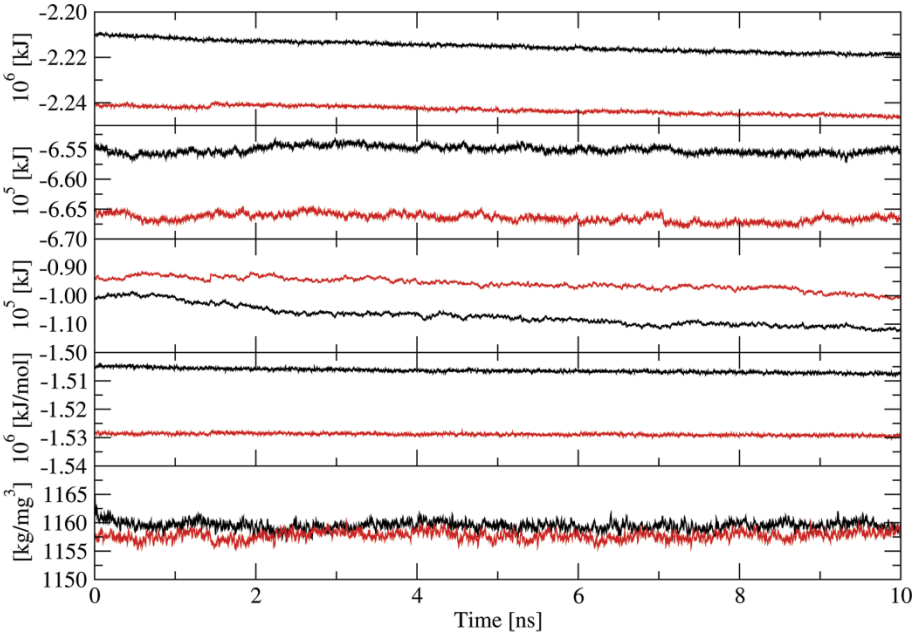

Figure 2. Time evolution of thermodynamics properties for the MD simulations corresponding to the aligned (black) and random (red) configurations of the LPS membrane. (A) Potential energy (kJ/mol); (B) solute potential energy (kJ/mol); (C) solute–solvent potential energy (kJ/mol); (D) density (kg/mg^3).

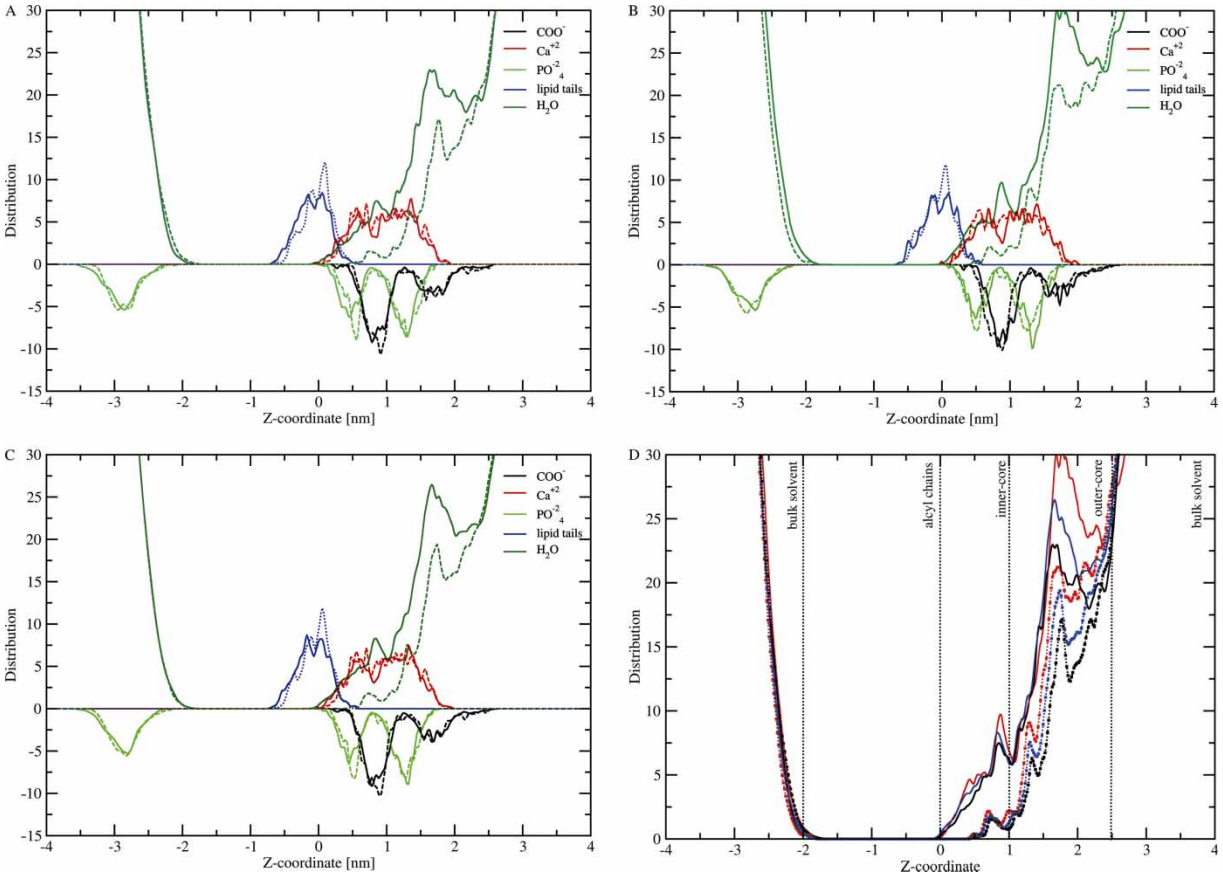

Figure 3. Distribution of functional groups along the axis normal to the LPS membrane surface. Values for the PO_4^{-2} and COO^- distributions are inverted for clarity. Group distributions along first 2.5 ns (A), final 2.5 ns (B), 10 ns of simulation (C). Aligned configuration system in bold line and random configuration system in dashed line. (D) Distribution of water molecules for the first 2.5 ns (black), final 2.5 ns (red) and 10 ns (blue) of simulation. Aligned configuration system in bold line and random configuration system represented by squares.

convergence of the solute–solvent interaction energy E_{SW} (Figure 2(D)). The dynamics of water molecules appears to be related to the presence of the divalent cations which has been shown to decrease the permeability of LPS–lipid bilayers [23,24] in part because water molecules compete with these cations for the same binding sites in the LPS outer and inner core [9,25]. The adequate reproduction of the diffusion dynamics of water molecules into the LPS membrane by the means of atomistic MD will certainly require simulations at much longer time scales.

The area per lipid molecule is a quantity difficult to measure directly from experiments [26–28]. It is usually inferred from other measurements such as carbon–deuterium order parameter S_{CD} of deuterated lipid tail atoms using ^{2}H NMR (Nuclear Magnetic Resonance) spectroscopy [27,29]. Reported measurements are scarce for LPS membranes and unavailable for the LPS membrane of *P. aeruginosa*. In this work, computational simulations will be compared against experimental measurements for experimental values for the area per LPS molecule that have been estimated for different LPS chemotypes of *Escherichia coli*, *Salmonella minnesota* and *Salmonella typhimurium* [24], as well as for PE [30], which forms the phospholipid inner layer of the LPS membrane. This procedure provides a reasonable assessment of the molecular model used to describe the LPS membrane and enables prediction of microscopic features currently unavailable for outer membranes of Gram-negative bacteria.

The average area per molecule was calculated from the cross-section of the simulation boxes divided by the 64 LPS and 160 lipid molecules and is illustrated in Figure 4 as a function of the simulation time. The average area per lipid molecule in the LPS_a and LPS_r simulations at 298.15 K was 0.428 ± 0.002 and 0.425 ± 0.001 nm^2, respectively. Although the convergence time varied for the two simulations, the corresponding average area per lipid in both simulations approaches the value of 0.43 nm^2 after 8 ns (Figure 4). Experimental average areas per lipid molecule for dilauroylphosphatidyl-ethanolamine at 293.15 K and at 308.15 K are 0.410

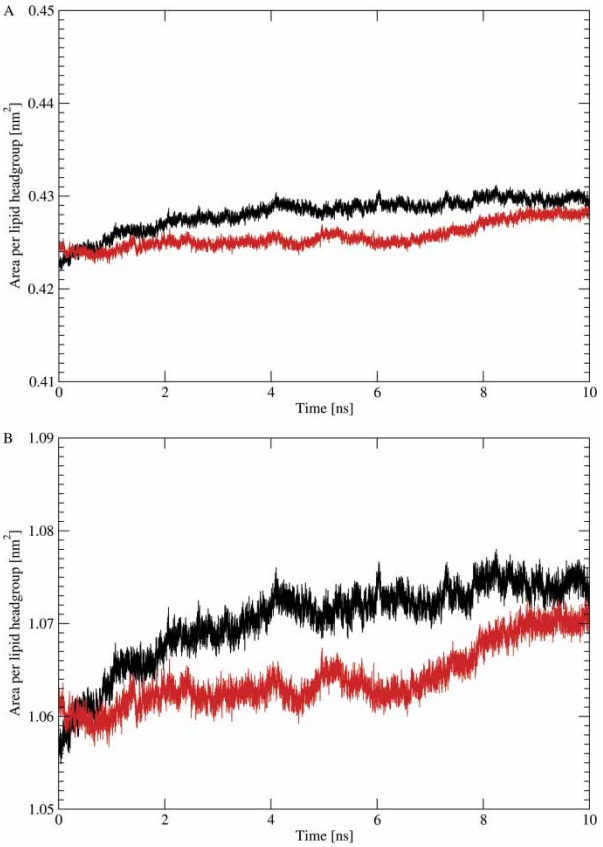

Figure 4. Area of per lipid molecule as function of time for (A) the PE phospholipid layer and (B) the Lipid-A layer in the aligned (black) and random (red) configurations of the LPS membrane.

and 0.512 nm^2, respectively [29], whereas for DPPE at 342.15 K, it is 0.55 nm^2, as calculated from order parameters of the CH_2 atoms near the head group (plateau region in the order parameter profile of the lipid tail) and shown to be the most suitable for inferring the area per lipid of a bilayer [26,27,30].

The average areas per LPS molecule calculated from the MD simulations are 1.08 ± 0.02 nm^2 for LPS_a and 1.06 ± 0.01 nm^2 for LPS_r. As for the area per lipid molecule, these values are equivalent for the two configurations. Experimental values for the area per LPS molecule have been inferred for different LPS chemotypes of *E. coli*, *S. minnesota* and *S. typhimurium* [24]. These values have been reported as area per carbon chain of 0.217 nm^2 at 293.15 K (gel–crystalline phase) and 0.260 nm^2 at 273.15 K (liquid–crystalline phase). For a penta-acyl LPS molecule, the respective areas per carbon chain will correspond to areas per LPS molecule of 1.085 and 1.300 nm^2. A certain degree of variation between calculated and experimental values for the area per LPS molecule is expected due to structural differences in the inner core and lipid-A regions of *P. aeruginosa* and the species for which the experimental measurements were performed [8]. *P. aeruginosa* has a larger total number of free OH groups per lipid-A molecule as well as the most highly phosphorylated inner core region among Gram-negative bacteria. These differences in the chemical composition greatly increase the number of hydrogen-bond sites in the LPS membrane of *P. aeruginosa*. As shown for PE and phosphatidyl-choline (PC) bilayers [31,32], the strong hydrogen-bond interactions between amine and phosphate and carbonyl groups of neighbouring PE molecules result in a significantly lower area per lipid for PE (0.55 nm^2 at 342.15 K) [30] with respect to PC (0.64 nm^2 at 323.15 K) [29]. A similar effect could explain the small differences between the experimental and calculated area per LPS molecule.

Carbon–deuterium order parameters S_{CD} for the PE lipid chains are presented in Table 2, together with experimental values at 342 K [30] and values from previous MD simulations of PE bilayers at 300 and 340 K [32]. S_{CD} values for the Lipid-A acyl chains were averaged over the initial and final 2.5 ns (Figure 5). In phospholipid bilayers, S_{CD} values remained relatively constant along the chain and then decreased near the end of the chain (Table 2). This profile is due to the tethering and alignment of the acyl segments near the aqueous interface, with increased disorder in the bilayer center due to the flexibility of the chain termini. S_{CD} values for the PE layer of the LPS membrane simulations at 298.15 K are similar to values obtained from previous simulations of the PE bilayer at 300 K, albeit higher than the experimental values for the PE bilayer at 342 K. However, calculated and experimental S_{CD} values for PE bilayers are comparable if obtained at the same temperature, *ca*. 340 K. This suggests that the deviation between calculated S_{CD} values for the LPS membrane and experimental ones for the phospholipids bilayer may be due to differences in temperature conditions.

The S_{CD} profiles for Lipid-A indicate moderately low order at the beginning of the acyl chains, then increase in the middle and decrease again at the end of the chains. A similar order parameter pattern has been reported for MD simulations of the monomeric form of ReLPS and Lipid-A molecules in solution [33,34]. Order parameters provide quantitative information about the degree of order along the lipid chain. Low order parameters typically result from the averaging of many different conformations of a methylene group under isotropic tumbling conditions, but they can also result from a fixed angle and thus low mobility. $S_{CD} = 0$ can be measured for an isotropically tumbling group in the NMR experiments as well as for a group fixed at an angle of 54.7°. The conformation of methylene groups near the disaccharide head group is influenced by their linkage to the *N*-acetyl-glucosamine backbone, which constrains their position at a fixed angle. These methylene groups are confined to an orientation resulting in low order

Table 2. Carbon–deuterium order parameters S_{CD} for acyl chains of the DPPE leaflet of the LPS membrane.

	Aligned configuration		Random configuration				
C-atom number	sn-2	sn-1	sn-2	sn-1	MD[§] 300 K	MD[§] 340 K	NMR[#] 342 K
1	0.30	0.30	0.31	0.28	0.30	0.26	0.23
2	0.35	0.31	0.34	0.29	0.31	0.26	0.23
3	0.36	0.32	0.35	0.31	0.33	0.26	0.23
4	0.36	0.29	0.35	0.28	0.35	0.24	0.23
5	0.35	0.15	0.33	0.13	0.36	0.25	0.23
6	0.31		0.29		0.36	0.24	0.23
7	0.26		0.23		0.36	0.24	0.23
8	0.09		0.08		0.35	0.23	0.23
9					0.35	0.22	0.23
10					0.34	0.20	0.20
11					0.33	0.19	0.18
12					0.32	0.17	0.15
13					0.30	0.15	0.13
14					0.25	0.11	0.10

Note: Values were calculated from 10-ns MD simulations of the aligned and random configurations of the LPS membrane at 298.15 K and compared against results from NMR spectroscopy at 342 K [30] and MD simulations of DPPE bilayers at 300 and 340 K [32]. Order parameters corresponding to DPPE bilayers were reported as average values between the sn1 and sn2 acyl chains.[§] From [32]. [#] From [30].

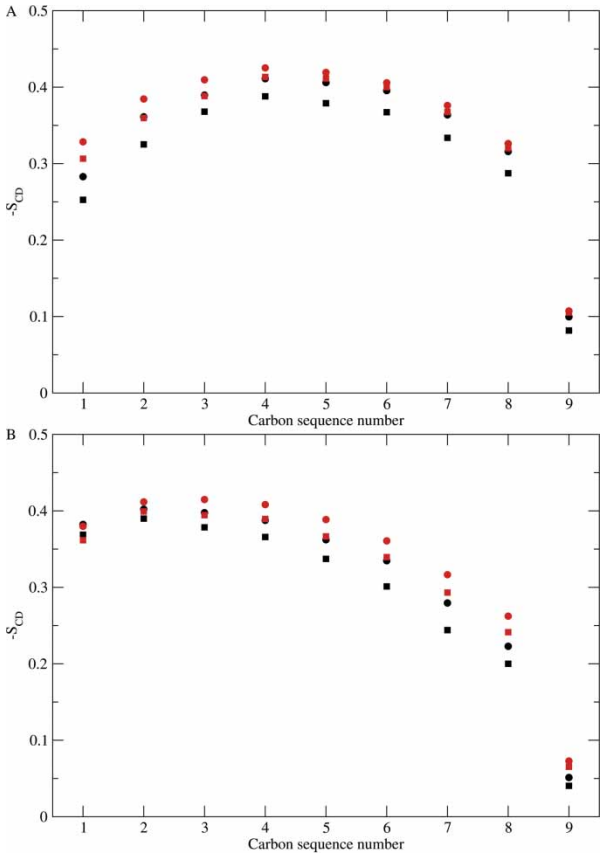

Figure 5. S_{CD} profiles for the acyl chains of the Lipid-A in the aligned (black) and random (red) configurations of the LPS membrane. A: chain I, B: chain II and C: chain III (see Figure 1 for acyl chain number assignments). Order parameter values were averaged over 64 LPS molecules and over different time windows: 0–2.5 ns (circle), 7.5–10 ns (square). Values are plotted as function of chain carbon number.

parameters [34]. The S_{CD} profiles are analogous in the two LPS simulations, without significant changes within the time period simulated (Figure 5). Differences between absolute S_{CD} values in the two ensembles of structures are very small, but consistent with the inverse relationship between lipid order parameters and the area per lipid molecule [27,35,36].

Calculated S_{CD} values are higher for the acyl chains of Lipid-A than for those of PE layer in the two LPS membrane simulations, indicating a more ordered hydrocarbon chains in the LPS leaflet. This is consistent with the experimental findings that acyl chains of Lipid-A in LPS membranes exhibit lower mobility than acyl chains in phospholipid bilayers, particularly in the presence of divalent cations [24,37–42] and that LPS membranes have higher melting temperatures (compared to phospholipids), which are further increased by the presence of Mg^{2+} and Ca^{2+} [2,37,43,44]. Indeed, comparative FTIR-spectroscopy studies for Lipid-A identified its melting temperature at 330.15 K, compared to 276.15 K for the phospholipid dioleoylglycerophosphate [2,37]. In the presence of divalent cations, melting temperatures of Lipid-A can reach values above 348.15 K [2,44]. Carboxylate and phosphate groups of the inner core and glycosamine backbone of the LPS membrane provide the binding sites for divalent cations [8,11,34]. The exceptionally high degree of phosphorylation observed in *P. aeruginosa* core is expected to result into even higher melting temperature and strongly ordered state hydrocarbon chains [2]. It should further be emphasised that because the conformation-dependent transition from an ordered, gel-like phase (β with all-trans packing of the acyl chains in Lipid-A) to a more fluid, disordered, liquid–crystalline phase (α with

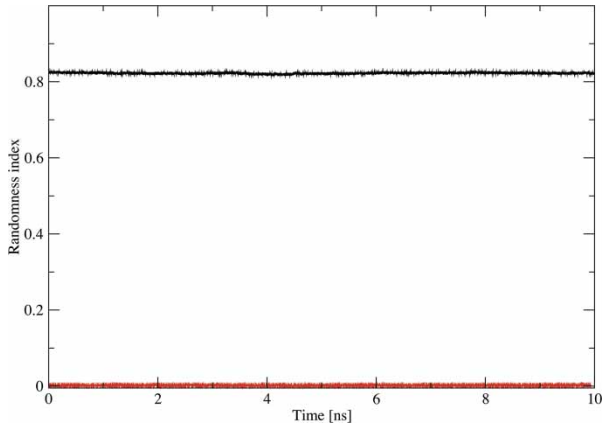

Figure 6. Cooperative orientation of the Lipid-A head groups in the LPS_a and LPS_r ensemble of structures quantitatively expressed by the randomness index $\bar{\chi}$.

gauche conformers present) occurs at temperatures above 323.15 K [24], under physiological conditions the LPS membrane will be in a gel-like state of very low fluidity [2]. The present MD simulations have been carried at a temperature of 298.15 K, where the acyl chain arrangement of LPS membrane is best described as in a gel–crystalline phase.

As a measure of the cooperative orientation of the Lipid-A head groups, a randomness index $\bar{\chi}$ was defined above. As is clear from the calculated values for the two simulations as a function of time as shown in Figure 6, both simulations retain their initial Lipid-A head group relative orientations throughout the 10 ns simulations. This index stays for the LPS_r simulation at a value close to zero as expected for a completely randomised set of head groups. For the LPS_a simulation some deviation from a perfectly aligned set of Lipid-A head groups occurred during setup and equilibration to a value of 0.8, which held constant during the production phase of the simulation. The observed values for $\bar{\chi}$ remain constant throughout both simulations, indicating that these simulations are 'locked' into the initial configurations, and that the lateral diffusion of the LPS is far beyond the time scale of these simulations. For this property the two simulations clearly did not converge.

3.3 Electrostatic properties

Due to the asymmetric nature of LPS membranes, a potential gradient arises from the higher surface charge density on the LPS side as compared with the PE side [45,46]. The distribution of electric charges across the membrane plays a crucial role in many membrane-related processes, from binding of charged species over insertion and orientation of integral membrane proteins to membrane transport phenomena like carrier transport and voltage-dependent gating of porin channels [46–48]. Studies *in vitro* of the porin PhoE in reconstituted planar bilayers composed of LPS on one side and phospholipids on the other shed light into the crucial role of the LPS matrix in the processes of folding [49], pore formation and channel gating [47] by outer membrane proteins. Therefore, an accurate description of the transmembrane potential in MD simulations of LPS membranes is highly desirable.

The electrostatic potential across the LPS membrane was calculated from the partial atomic charges used in the simulations for a total of 5000 structures regularly sampled along the respective LPS_a and LPS_r trajectory files. The average transmembrane electrostatic potential in both simulations is found to be around -130 mV (Figure 7(A)). Comparison of the transmembrane electrostatic potential along time for the LPS_a and LPS_r simulations shows convergence after 6 ns (Figure 7(B)). The membrane potential of reconstituted planar bilayers composed of LPS and phospholipids can be estimated by the means of the Gouy–Chapman formalism (diffuse

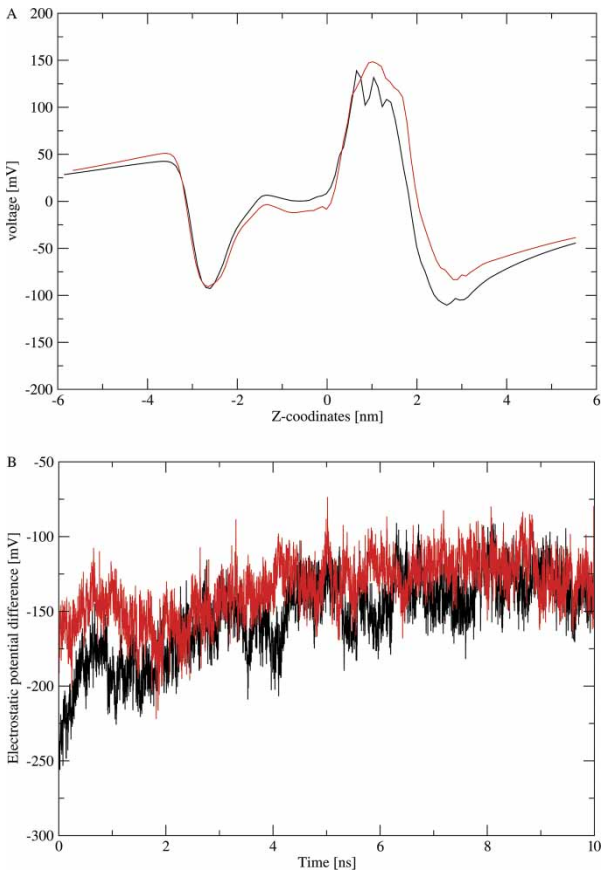

Figure 7. Transmembrane electrostatic potential for the aligned (black) and random (red) configuration of the LPS membrane. Electrostatic potential values were calculated for 5000 structures from 2-ps interval averages throughout 10 ns of simulations. (A) Average transmembrane electrostatic potential along 10 ns of simulation. (B) Potential difference across the axis normal to the LPS membrane surface versus time.

double-layer theory) [45,50,51]. These membrane potentials can then be probed with carrier-ion complexes via the measurement of current/voltage characteristics. Previously reported values of membrane potential for *Paracoccus denitrificans* and *S. minnesota* are −74 and −85 mV, respectively [46,48]. These values are of the same sign and order of magnitude as the transmembrane electrostatic potential values obtained from the MD simulations. It is important to be cautions in comparing these values because of significant differences in the theoretical approaches used to estimate these potentials. In the diffuse double-layer model used, the membrane has a uniform charge density in an electrolyte solution with the interior and exterior of the membrane continuum described by different dielectric constants [46,48]. Therefore, the magnitude of the surface potential at the membrane surface will depend on the surface charge density, the kinds of electrolytes and their concentration. Conversely, due to the atomistic nature of the MD simulations, the transmembrane electrostatic potential estimated from the corresponding trajectories accounts for a highly non-uniform charge distribution as well as for the conformational dynamics of the membrane. Furthermore, the reconstituted planar bilayers are composed of LPS and a mixture of phospholipids, namely phosphatidylglycerol and diphosphatidylglycerol, which at neutral pH will carry one and two charges per molecule, respectively. In our simulations, the PE layer is neutral. Third, the chemical composition of the LPS in *P. aeruginosa* differs with respect to *P. denitrificans* and *S. minnesota*. *P. aeruginosa* has the most highly phosphorylated inner core region among Gram-negative bacteria which could account for a more electronegative surface potential.

4. Conclusion

In the present work, MD simulations of two different configurations of an outer membrane slab formed by 64 LPS and 140 DPPE molecules in explicit solvent were performed aiming to validate model-derived properties against the available experimental data, identify the properties whose dynamics can be sampled on nanosecond timescales, and evaluate the dependence of the convergence of structural and dynamical properties on the initial configuration of the system, within the chosen force field and simulation conditions. It was found that the two initial configurations do not converge to a common ensemble of configuration in the time scale of the simulations, and that the lateral diffusion of the LPS is far beyond these time scales. Likewise, water permeation into the LPS membrane was found to require significantly longer simulations.

The outer membrane of Gram-negative bacteria differs in many physiological and biochemical properties from the cytoplasmic membrane. Although their lipid content is similar, their proteins are different, and only the outer membrane contains LPS. The biological properties of outer membranes such as low permeability, intrinsic antibiotic resistance and immunogenicity are thought to depend on LPS structure, aggregation and packing properties [1,37,52–55]. These properties will also influence the stability of and mediate transport across outer membrane proteins. Compared to typical phospholipid bilayers, LPS membranes have tighter hydrocarbon chain packing that may play a critical role in its barrier properties [24,41,42,53]. Moreover, the chemical structure of LPS confers an asymmetric character to outer membranes that has been shown to play an important role in the electrical properties of porins [2,8,47]. Therefore, an accurate description of the behaviour and function of outer membrane proteins relevant for *in vivo* conditions will immensely benefit from a more realistic model that accounts for the high asymmetry and low fluidity characteristics of outer membranes [14].

While a number of properties did not reach convergence in a nanosecond simulation times, these are predominantly related to the slow lateral diffusion of the LPS molecules within the outer leaflet of the outer membrane. On the other hand, this study shows that characteristics of the outer membrane that will significantly impact the structural and internal dynamics of transmembrane proteins, most notably the electrostatic potential and molecular density, do converge within the time scale accessible by computer simulation. This is especially encouraging for the study of the energetic and dynamical properties of membrane proteins in their natural environment.

Acknowledgements

This research was supported in part by NIH, National Institute for Allergy and Infectious Diseases. Development of the large-scale trajectory analysis required for this project was supported by the Data Intensive Computing for complex biological systems project funded by the Department of Energy Office of Advanced Scientific Computing Research. The authors acknowledge the use of computational resources provided by the William R. Wiley Environmental Molecular Sciences Laboratory. Dr Roberto D. Lins is acknowledged for critical reading of the manuscript. Pacific Northwest National Laboratory is operated for the Department of Energy by Battelle.

References

[1] K. Brandenburg and A. Wiese, *Endotoxins: relationships between structure, function, and activity*, Curr. Top. Med. Chem. 4 (2004), p. 1127.

[2] H. Nikaido, *Molecular basis of bacterial outer membrane permeability revisited*, Microbiol. Mol. Biol. Rev. 67 (2003), p. 593.

[3] R.S. Munford, *Severe sepsis and septic shock: the role of Gram-negative bacteremia*, Annu. Rev. Pathol. Mech. Dis. 1 (2006), p. 467.

[4] C. Erridge, E. Bennett-Guerrero, and I.R. Poxton, *Structure and function of lipopolysaccharides*, Microb. Infect. 4 (2002), p. 837.

[5] G.B. Pier, *Promises and pitfalls of* Pseudomonas aeruginosa *lipopolysaccharide as a vaccine antigen*, Carbohydr. Res. 338 (2003), p. 2549.

[6] L.L. Burrows and J.S. Lam, *Effect of wzx(rfbX) mutations on A-band and B-band lipopolysaccharide biosynthesis in* Pseudomonas aeruginosa *O5*, J. Bacteriol. 181 (1999), p. 973.

[7] I. Sadovskaya *et al.*, *Elucidation of the lipopolysaccharide core regions of the wild-type strain PAO1 and* O*-chain-deficient mutant strains AK1401 and AK1012 from* Pseudomonas aeruginosa *serotype O5*, Eur. J. Biochem. 255 (1998), p. 673.

[8] S.G. Wilkinson, *Bacterial lipopolysaccharides – themes and variations*, Prog. Lipid Res. 35 (1996), p. 283.

[9] T. Abraham *et al.*, *Neutron diffraction study of* Pseudomonas aeruginosa *lipopolysaccharide bilayers*, J. Phys. Chem. B 111 (2007), p. 2477.

[10] T.A. Soares, X. Daura, C. Oostenbrink, L.J. Smith, and W.F. Van Gunsterin, *Validation of the* GROMOS *force field parameter set 45A3 against nuclear magnetic resonance data of hen egg lysozyme*, J. Biomol. NMR 30 (2004), p. 407.

[11] R.D. Lins and T.P. Straatsma, *Computer simulation of the rough lipopolysaccharide membrane of* Pseudomonas aeruginosa, Biophys. J. 81 (2001), p. 1037.

[12] M. Schindler, M.J. Osborn, and D.E. Koppel, *Lateral diffusion of lipopolysaccharide in the outer membrane of* Salmonella typhimurium, Nature 285 (1980), p. 261.

[13] K. Gawrisch, *The dynamics of membrane lipids*, in *The Structure of Biological Membranes*, P.L. Yeagle, ed., CRC Press, Boca Raton, FL, 2005, pp. 147–171.

[14] M. Baaden and M.S.P. Sansom, *OmpT: Molecular dynamics simulations of an outer membrane enzyme*, Biophys. J. 87 (2004), p. 2942.

[15] S. Khalid *et al.*, *Modeling and simulations of a bacterial outer membrane protein: OprF from* Pseudomonas aeruginosa, Proteins: Struct. Funct. Bioinf. 63 (2006), p. 6.

[16] H.J.C. Berendsen, J.R. Grigera, and T.P. Straatsma, *The missing term in effective pair potentials*, J. Phys. Chem. B 91 (1987), p. 6269.

[17] R.W. Hockney, *The potential calculation and some applications*, in *Methods in Computational Physics*, B. Alder, S. Fernbach, and M. Rotenberg, eds., Academic Press, New York, NY, 1970, pp. 135–211.

[18] H.J.C. Berendsen *et al.*, *Molecular-dynamics with coupling to an external bath*, J. Chem. Phys. 81 (1984), p. 3684.

[19] J.P. Ryckaert, G. Ciccotti, and H.J.C. Berendsen, *Numerical integration of the cartesian equations of motion of a system with constraints: molecular dynamics of* n*-alkanes*, J. Comp. Phys. 23 (1977), p. 327.

[20] U. Essmann *et al.*, *A smooth particle mesh Ewald method*, J. Chem. Phys. 103 (1995), p. 8577.

[21] T.P. Straatsma, M. Philippopoulos and J.A. McCammon, *NWChem: exploiting parallelism in molecular simulations*, Comp. Phys. Comm. 128 (2000), p. 377.

[22] T.P. Straatsma and T.A. Soares, *Data intensive analysis of biomolecular simulations*, International Conference of Computational Methods in Sciences and Engineering. American Institute of Physics Proceedings Corfu, Greece, 2007.

[23] P. Garidel *et al.*, *Divalent cations affect chain mobility and aggregate structure of lipopolysaccharide from* Salmonella minnesota *reflected in a decrease of its biological activity*, Biochim. Biophys. Acta Biomembr. 1715 (1999), p. 122.

[24] S. Snyder, D. Kim, and T.J. McIntosh, *Lipopolysaccharide bilayer structure: effect of chemotype, core mutations, divalent cations, and temperature*, Biochemistry 38 (1999), p. 10758.

[25] F.G. Ferris and T.J. Beveridge, *Physicochemical roles of soluble metal-cations in the outer-membrane of* Escherichia coli *K-12*, Can. J. Microbiol. 32 (1986), p. 594.

[26] J.F. Nagle, *Area lipid of bilayers from NMR*, Biophys. J. 64 (1993), p. 1476.

[27] H.I. Petrache, S.W. Dodd, and M.F. Brown, *Area per lipid and acyl length distributions in fluid phosphatidylcholines determined by H-2 NMR spectroscopy*, Biophys. J. 79 (2000), p. 3172.

[28] H.I. Petrache, K.C. Tu, and J.F. Nagle, *Analysis of simulated NMR order parameters for lipid bilayer structure determination*, Biophys. J. 76 (1999), p. 2479.

[29] J.F. Nagle and S. Tristram-Nagle, *Structure of lipid bilayers*, Biochim. Biophys. Acta Biomembr. 1469 (2000), p. 159.

[30] R.L. Thurmond, S.W. Dodd, and M.F. Brown, *Molecular areas of phospholipids as determined by 2H NMR spectroscopy*, Biophys. J. 59 (1991), p. 108.

[31] A. Blume *et al.*, *Phase equilibria, molecular conformation, and dynamics in phosphatidylcholine phosphatidylethanolamine bilayers*, Biochemistry 21 (1982), p. 6243.

[32] S. Leekumjorn and A.K. Sum, *Molecular simulation study of structural and dynamic properties of mixed DPPC/DPPE bilayers*, Biophys. J. 90 (2006), p. 3951.

[33] V. Frecer, B. Ho, and J.L. Ding, *Molecular dynamics study on lipid A from* Escherichia coli*: insights into its mechanism of biological action*, Biochim. Biophys. Acta 1466 (2000), p. 87.

[34] S. Obst, M. Kastowsky, and H. Bradaczek, *Molecular dynamics simulations of six different fully hydrated monomeric conformers of* Escherichia coli *re-lipopolysaccharide in the presence and absence of* Ca^{+2}, Biophys. J. 72 (1997), p. 1031.

[35] H. Schindler and J. Seelig, *Deuterium order parameters in relation to thermodynamics properties of a phospholipid bilayer – statistical mechanical interpretation*, Biochemistry 14 (1975), p. 2283.

[36] J. Seelig and A. Seelig, *Deuterium magnetic-resonance studies of phospholipid bilayers*, Biochem. Biophys. Res. Commun. 57 (1974), p. 406.

[37] K. Brandenburg and U. Seydel, *Investigation into the fluidity of lipopolysaccharide and free lipid A membrane systems by Fourier-transform infrared spectroscopy and differential scanning calorimetry*, Eur. J. Biochem. 191 (1990), p. 229.

[38] S. Cheng, J.K. Thomas, and C.F. Kulpa, *Dynamics of pyrene fluorescence in* Escherichia coli *membrane-vesicles*, Biochemistry 13 (1974), p. 1135.

[39] S. Rottem, M. Hasin, and S. Razin, *Outer membrane of* Proteus mirabilis *2. Extractable lipid fraction and electron-paramagnetic resonance analysis of outer and cytoplasmic membranes*, Biochim. Biophys. Acta 375 (1975), p. 395.

[40] S. Rottem and L. Leive, *Effect of variation in lipopolysaccharide on the fluidity of the outer membrane of* Escherichia coli, J. Biol. Chem. 252 (1977), p. 2077.

[41] D. Allende and T.J. McIntosh, *Lipopolysaccharides in bacterial membranes act like cholesterol in eukaryotic membranes in providing protection against melittin-induced bilayer lysis*, Biochemistry 42 (2003), p. 1101.

[42] S. Snyder and T.J. McIntosh, *The lipopolysaccharide barrier: Correlation of antibiotic susceptibility with antibiotic permeability and fluorescent probe binding kinetics*, Biochemistry 39 (2000), p. 11777.

[43] D.L. Melchior and J.M. Steim, *Thermotropic transitions in biomembranes*, Annu. Rev. Biophys. Bioeng. 5 (1976), p. 205.

[44] H. Nikaido *et al.*, *Outer membrane of* Salmonella typhimurium *– electron-spin resonance studies*, Biochim. Biophys. Acta 465 (1977), p. 152.

[45] S.O. Hagge *et al.*, *Inner field compensation as a tool for the characterisation of asymmetric membranes and peptide–membrane interactions*, Biophys. J. 86 (2004), p. 913.

[46] U. Seydel *et al.*, *Electrostatic potential barrier in asymmetric planar lipopolysaccharide/phospholipid bilayers probed with the valinomycin-*K^+ *complex*, Z. Naturforsch. C 42 (1992), p. 757.

[47] S.O. Hagge *et al.*, *Pore formation and function of phosphoporin PhoE of* Escherichia coli *are determined by the core sugar moiety of lipopolysaccharide*, J. Biol. Chem. 277 (2001), p. 34247.

[48] A. Wiese *et al.*, *Influence of the lipid matrix on incorporation and function of LPS-free porin from* Paracoccus denitrificans, Biochim. Biophys. Acta 1190 (1994), p. 231.

[49] H. De Cock *et al.*, *Non-lamellar structure and negative charges of lipopolysaccharides required for efficient folding of outer membrane protein PhoE of* Escherichia coli, J. Biol. Chem. 271 (1999), p. 5114.
[50] J.N. Israelachvili, *Intermolecular and Surface Forces*. Academic Press, New York, NY, 1992.
[51] S. Ohki and R.A. Spangler, *Passive and facilitated transport*, in *The Structure of Biological Membranes*, P.L. Yeagle, ed. CRC Press, Boca Raton, FL, 2005, pp. 329–387.
[52] K. Brandenburg, *Fourier transform infrared spectroscopy characterisation of the lamellar and nonlamellar structures of free lipid A and Re lipopolysaccharides from* Salmonella minnesota *and* Escherichia coli, Biophys. J. 64 (1993), p. 1215.
[53] H. Labischinski *et al.*, *High state of order of isolated bacterial lipopolysaccharide and its possible contribution to the permeation barrier property of the outer membrane*, J. Bacteriol. 161 (1985), p. 9.
[54] C.R.H. Raetz and C. Whitfield, *Lipopolysaccharide endotoxins*, Annu. Rev. Biochem. 71 (2002), p. 635.
[55] E.T. Rietschel *et al.*, *Bacterial endotoxin: Molecular relationships of structure to activity and function*, FASEB J. 8 (1994), p. 217.